

## GOLDSTONE BOSONS AND FINITE SIZE EFFECTS: A NUMERICAL STUDY OF THE O(4) MODEL

A. HASENFRATZ<sup>1</sup>, K. JANSEN<sup>2</sup>, J. JERSÁK<sup>2,3</sup>, H.A. KASTRUP<sup>3</sup>, C.B. LANG<sup>4</sup>,  
H. LEUTWYLER<sup>5</sup> and T. NEUHAUS<sup>6</sup>

<sup>1</sup>*Department of Physics, University of Arizona, Tucson, AZ 85721, USA*

<sup>2</sup>*HLRZ c/o KFA Jülich, P.O. Box 1913, W-5170 Jülich, Germany*

<sup>3</sup>*Institut für Theoretische Physik, RWTH Aachen, W-5100 Aachen, Germany*

<sup>4</sup>*Institut für Theoretische Physik, Universität Graz, A-8010 Graz, Austria*

<sup>5</sup>*Institut für Theoretische Physik, Universität Bern, CH-3012 Bern, Switzerland*

<sup>6</sup>*Fakultät für Theoretische Physik, Universität Bielefeld, W-4800 Bielefeld, Germany*

Received 5 July 1990

We study the 4-component  $\Phi^4$  model in 4 dimensions in the broken phase where the Goldstone modes dominate the finite size effects. Chiral perturbation theory relates the quantities measured at non-vanishing external source and in a finite volume to the low energy parameters  $\Sigma$  (the field expectation value) and  $F$  (the pion decay constant) defined at infinite volume in the limit of vanishing external source. We analyze high statistics Monte Carlo data for the field expectation value and the Goldstone propagator by means of such expansions and we find very good agreement with the theoretically expected functional behaviour. It is possible to identify non-leading terms in the finite volume expansion and determine corresponding scale parameters. We also explore some alternative methods applicable at vanishing external source. Our analysis demonstrates that in a situation where the light Goldstone bosons control the dynamics of the system at large distances one may determine the infinite volume, zero external source quantities from finite volume simulations in a theoretically controlled way.

### 1. Introduction

Many recent non-perturbative studies of the Higgs mechanism in the standard model concentrated on the investigation of the O(4)-symmetric scalar sector in the broken symmetry phase, following a suggestion of Dashen and Neuberger [1]. This simplification is supported by the observation [2] that weakly coupled gauge fields do not change the non-interacting character of the  $\Phi^4$  theory. (For recent reviews on these subjects cf. refs. [3–6].) However, for heavy Higgs bosons the effective renormalized quartic coupling may be large and a non-perturbative control of the scalar sector is essential.

Non-perturbative analytic investigations of the scalar sector either in the continuum using a momentum cut-off [7] or on the hypercubic lattice [8], as well as several numerical Monte Carlo studies on hypercubic lattices [9–13] find that,

actually, the scalar sector is not strongly interacting and that the Higgs boson mass cannot exceed the upper bound  $m_H < 640$  GeV. This result may depend on the adopted regularization scheme and therefore an investigation of the scalar field theory on various types of lattices is required [14–17]. Methods for comparing the results obtained by means of different regularization schemes are being developed [4, 16–18]; they require calculations of high precision in a region of the coupling parameter space where the universal asymptotic scaling associated with the (“trivial”) gaussian fixed point sets in.

All Monte Carlo results are obtained on lattices with finite size and have to be extrapolated to infinite volume. This requires a detailed analytic understanding of the volume dependence in order to allow a reliable extrapolation. In the symmetric phase of the O(4)-symmetric  $\Phi^4$  theory the finite size effects could be controlled [19] by means of lattice perturbation theory [20]. In the phase with the spontaneously broken O(4) symmetry the finite size effects are of two types:

(i) Long range correlation associated with the small mass of the Goldstone bosons;

(ii) Finite size effects from the massive component (Higgs boson, here called the  $\sigma$ -particle) where the correlation length associated with its mass,  $\xi_\sigma = 1/M_\sigma$ , is comparable with a characteristic lattice size  $L$ .

Both effects coexist and may lead to a very complex dependence of various observables on the lattice size. The understanding of the second one certainly requires, as a first step, a good control of the finite size effects caused by the Goldstone bosons alone\*.

This is the reason why in this paper we concentrate on the finite size effects related to the Goldstone bosons under the condition that the finite size effects caused by the  $\sigma$ -particle are negligible,

$$M_\sigma \gg \frac{1}{L}. \quad (1.1)$$

In studies of some models in statistical mechanics [23, 24], of chromodynamics [25–28] and of the Higgs sector [29] it has been argued that the Goldstone boson related finite size effects are of a universal character, determined by the symmetries of the dynamics in terms of a few low energy constants and by the geometry of the finite system. Here, we use the theory of these finite size effects as developed

\* We note that at present the finite size effects of the Goldstone bosons, which are the would-be longitudinal components of the massive gauge bosons when the gauge coupling is switched on, cannot be avoided by including the gauge fields, though some reasonable estimates for the upper bound on the Higgs boson mass have been obtained in the SU(2) lattice Higgs model [21]. Indeed, considerable finite size effects have been observed in the lattice Higgs models even at relatively large gauge coupling [22] and their theoretical control is not yet in sight.

in an effective lagrangian approach [25–28,30]. The effective lagrangian has the same symmetry as the original system but is simple enough to allow a *systematic* perturbative expansion. In systems of finite size  $L$  this amounts to an expansion in powers of  $L^{-2}$ . The expansion is reliable because the interaction between the Goldstone modes is weak at low momenta.

The first application of this theory [25,26] has been made in the context of the study of finite size effects in QCD with light quarks, whose low energy properties are determined by the chiral  $SU(2) \otimes SU(2) \simeq O(4)$  symmetry [31]. Therefore we refer to this approach here as “chiral perturbation theory”, too. A comprehensive description can be found in several recent papers [27,28,30]. Its low order terms depend only on two parameters  $\Sigma$  and  $F$ , which in QCD have the physical meaning of the quark condensate and of the pion decay constant, respectively.

In this paper we want to test numerically the applicability and accuracy of chiral perturbation theory for finite size effects in the scalar sector of the electroweak theory. In particular, we want to determine the low energy constants  $\Sigma$  and  $F$  with good precision. In the present context these correspond to the vacuum expectation value of the scalar field and to  $F = \Sigma / \sqrt{Z}$ , where  $Z$  is the wave function renormalization constant. The knowledge of  $F$  is required for a perturbative calculation of the vector boson mass in the standard model. We do not study the mass  $M_\sigma$  of the  $\sigma$ -particle here, because the control of the finite size effects for this quantity requires methods beyond the effective lagrangian approach (for some results in this direction cf. [13]).

The present work is a continuation of our systematic application of chiral perturbation theory for a control of finite size effects in the numerical study of the  $O(4) \Phi^4$  theory, initiated in ref. [11] and continued in ref. [32]. Related work has been done also by Heller and Neuberger [33]. We extend the promising results of ref. [32] by taking into account one additional order of the chiral perturbation expansion and by including more data closer to the phase transition as well as some data obtained on asymmetric lattices. Some of these results have been reported in a preliminary form in ref. [34].

The notation for the model is clarified in sect. 2. In sect. 3 the finite size effects due to Goldstone modes are discussed qualitatively and, following refs. [25,30], two types of expansions are introduced together with the expected domains of validity. The relevant expressions for the field expectation value and the Goldstone correlation function in both domains are given. Sect. 4 is concerned with the numerical method. Here we give an account of our data and discuss the error analysis and checks on the consistency of the data.

The results for a non-vanishing external source (sect. 5) are organized, according to the presentation in sect. 3, into parts on the field expectation value and the Goldstone boson propagator. Sect. 6 deals with results obtained for a vanishing external source for the susceptibility in a hypercubic geometry and the propagators in a cylinder geometry, utilizing ideas presented recently [26,28,34,35].

## 2. The model and the low energy constants at infinite volume

The lattice regularized action for the scalar sector of the standard model is

$$S = -2\kappa \sum_{x \in \Lambda} \sum_{\mu=1}^4 \Phi_x^\alpha \Phi_{x+\mu}^\alpha + \lambda \sum_{x \in \Lambda} (\Phi_x^\alpha \Phi_x^\alpha - 1)^2 + \sum_{x \in \Lambda} \Phi_x^\alpha \Phi_x^\alpha - J \sum_{x \in \Lambda} \Phi_x^0, \quad (2.1)$$

where  $\kappa, \lambda \geq 0$  are the bare hopping and quartic coupling parameters, respectively. The field has four real components  $\Phi^\alpha$  with  $\alpha = 0, 1, 2, 3$ . It is convenient to introduce the external source  $J$  which allows a proper definition of spontaneous symmetry breaking. Its use is of crucial importance in chiral perturbation theory. The normalization of the field and the external source used in the continuum is obtained by the rescaling

$$\varphi^\alpha \equiv \sqrt{2\kappa} \Phi^\alpha, \quad j \equiv \frac{J}{\sqrt{2\kappa}}. \quad (2.2)$$

The non-perturbative investigation of the scalar sector of the electroweak theory is of most interest at  $\lambda = \infty$  where the renormalized quartic coupling has the largest value for a fixed  $M_\sigma$  [8, 9, 11]; the upper bound on the Higgs boson mass is obtained for this value of  $\lambda$ . For tests of the chiral perturbation theory this choice of  $\lambda$  should be as good as any other. Therefore we have performed all our calculations for infinite  $\lambda$ , for which the model (2.1) is described by the action

$$S = -2\kappa \sum_{x \in \Lambda} \sum_{\mu=1}^4 \Phi_x^\alpha \Phi_{x+\mu}^\alpha - J \sum_{x \in \Lambda} \Phi_x^0, \quad \Phi_x^\alpha \Phi_x^\alpha = 1. \quad (2.3)$$

In this non-linear  $\sigma$ -model the critical point is for  $J = 0$  at  $\kappa = \kappa_c = 0.3045(7)$  [11].

At infinite volume, O(4) symmetry is spontaneously broken for sufficiently large  $\kappa$ . In this phase

$$\langle \varphi_x^0 \rangle = \Sigma; \quad \langle \varphi_x^i \rangle = 0 \quad (i = 1, 2, 3). \quad (2.4)$$

Here the spectrum of the theory contains three massless Goldstone bosons corresponding to the excitations in the O(4) directions  $\alpha = i = 1, 2, 3$ . Therefore, the correlation functions do not fall off exponentially at large distances, but with an inverse power of the distance. Specifically, the Goldstone boson two-point function  $\langle \varphi_x^i \varphi_y^j \rangle$  satisfies

$$\lim_{|x-y| \rightarrow \infty} 4\pi^2 |x-y|^2 \langle \varphi_x^i \varphi_y^j \rangle = Z \delta^{ij}. \quad (2.5)$$

The quantity  $Z$  is the wave function renormalization constant and the renormalized fields are  $\varphi_x^\alpha/\sqrt{Z}$ .

The model contains six currents, all conserved at  $J = 0$ , whose charges generate the group  $O(4)$ . The corresponding Ward identities strongly constrain the behaviour of the correlation functions at large distances. In fact, the asymptotic behaviour of all the Green functions associated with the currents and with the fields  $\varphi_x^\alpha$  is determined by the two low energy constants  $\Sigma$  and  $F$  [31]. The first of these constants is the vacuum expectation value of the scalar field, defined in eq. (2.4). The second one specifies the matrix elements of the axial currents  $A_\mu^j(x) = \varphi^j \partial_\mu \varphi^0 - \varphi^0 \partial_\mu \varphi^j$  (in Minkowski space) between the ground state and single Goldstone boson states

$$\langle 0 | A_\mu^j(0) | \pi^k(p) \rangle = i \delta^{jk} p_\mu F. \quad (2.6)$$

In analogy with QCD, the constant  $F$  is often referred to as the pion decay constant. The low energy constants  $Z$ ,  $\Sigma$  and  $F$  are related through

$$\Sigma = F \sqrt{Z}. \quad (2.7)$$

For  $J > 0$  the Goldstone boson mass  $M_\pi$  has a non-vanishing value which in the lowest order of chiral perturbation theory is

$$M_\pi^2 = j \frac{\Sigma}{F^2}. \quad (2.8)$$

In higher orders of the chiral perturbation theory some further low energy constants  $\Lambda_\Sigma$ ,  $\Lambda_F$  and  $\Lambda_M$  are required [30]. They are the scale parameters determining the logarithmic dependence of  $\Sigma$ ,  $F$  and  $M_\pi$  on  $j$ .

### 3. Finite volume effects due to Goldstone bosons

#### 3.1. SCALES OF THE FINITE SIZE EFFECTS AND THE RESTORATION OF SYMMETRY

Let us now consider the model (2.1) in a finite volume

$$V = L_s^3 L_t \equiv L^4, \quad (3.1)$$

where  $L_s$  and  $L_t$  are of the same order of magnitude and  $L$  is the characteristic size of the system. At finite volume spontaneous symmetry breaking cannot occur. The properties of the field expectation values and correlation functions are qualitatively different: at finite volume, the Goldstone bosons generate large finite size effects, even if the volume is large. This confronts Monte Carlo calculations

with a problem of principle: to determine the properties of the system at infinite volume from the measurements performed at finite volume.

In some of our earlier studies of the model (2.1) at  $J = 0$  [9, 11] we determined the absolute value of the field, normalized to the volume, for each configuration separately and estimated  $\Sigma$  by the expectation value<sup>\*</sup>,

$$\Sigma = \langle |\bar{\varphi}^\alpha| \rangle, \quad \bar{\varphi}^\alpha = \frac{1}{V} \sum_x \varphi_x^\alpha. \quad (3.2)$$

Similar techniques have been used also in refs. [10, 33]. The reliability of this method will be tested in this paper and is currently also under analytic investigation [35].

The constant external source  $j$  breaks the  $O(4)$  symmetry explicitly, in analogy to a constant external magnetic field. In chiral perturbation theory, for small values of  $j$ , the qualitative properties of the system at large volume are controlled by the  $j$ -dependent part  $u_0$  of the classical action of a configuration with a “magnetization”  $\Sigma$ ,

$$u_0 = \Sigma j L^4. \quad (3.3)$$

If this parameter is small compared to 1, then the expectation value of the field is small and the correlation functions are approximately  $O(4)$ -symmetric.

For  $j$  fixed and growing volume, we eventually reach the region  $u_0 \gg 1$ , where the expectation value of the field approximates the infinite volume value. The external source provides a continuous interpolation between these two qualitatively different domains of small and large symmetry breaking [23, 24].

In order for the finite size effects to be controlled by the symmetry properties of the model, two conditions should be satisfied:

(i) First, as expressed by the inequality (1.1), the box must be large compared to the Compton wavelength  $M_\sigma^{-1}$  of the  $\sigma$ -particle.

(ii) Second, the mass of the Goldstone bosons should be small compared to  $M_\sigma$ , which can be expressed, by means of eq. (2.8), as an upper limit on the magnitude of the external source

$$M_\pi^2 \ll M_\sigma^2, \quad \text{i.e.} \quad j \ll M_\sigma^2 F^2 / \Sigma. \quad (3.4)$$

Thus if the volume is large and if the source is small, the dominant dependence of the expectation values and correlation functions on  $V$  and on  $j$  is determined by the low energy constants  $\Sigma$  and  $F$  which characterize the asymptotic behaviour of the correlation functions at infinite volume [23–25]. Further parameters enter only in higher orders of the chiral perturbation expansion [30].

<sup>\*</sup> In refs. [9, 11] the quantity  $\bar{\varphi}^\alpha$  has been denoted  $M^\alpha$ .

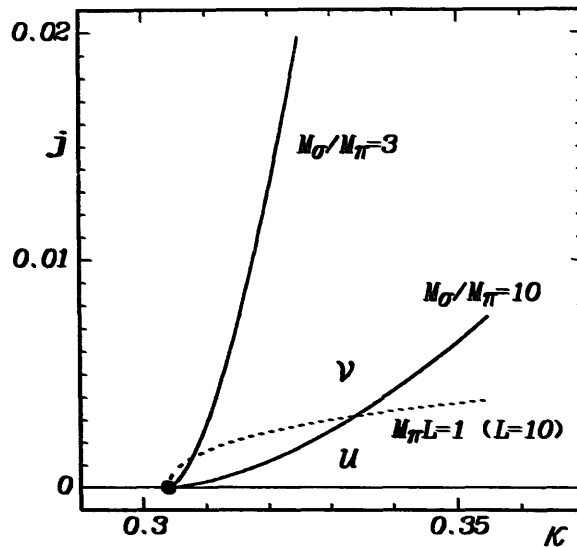


Fig. 1. Lines of constant  $M_\sigma/M_\pi$  in the  $\kappa$ - $j$  plane. The dashed line is a line  $M_\pi L = 1$  on a  $10^4$  lattice. The regions below (above) the dashed line are the  $\mathcal{U}$  ( $\mathcal{V}$ ) domains for  $L = 1$ .

Let us illustrate the meaning of the condition (3.4): in fig. 1 we show in the  $\kappa$ - $j$  plane the lines of constant ratios  $M_\sigma/M_\pi = 1/3$  and  $1/10$  (solid lines), as obtained from the scaling laws [36] for  $M_\sigma$  and  $\Sigma$  with the coefficients fixed by the data. In the regions below the upper (lower) line chiral perturbation theory is expected to be applicable with reasonable (excellent) reliability. In practice the condition (3.4) turns out not to be very stringent, because even for ratios  $M_\pi/M_\sigma \leq 1$  the non-leading terms in the expansions can be quite small, indicating a good convergence. However, this has to be checked in each case individually, in particular in the vicinity of the critical point. To provide such practical insights is one of the motivations of our study.

The effects of the  $\sigma$ -particle should be local if the conditions (1.1) and (3.4) are met. The expectation values and correlation functions at distances  $t$  satisfying

$$t \gg \frac{1}{M_\sigma}, \quad (3.5)$$

can then be expanded systematically in powers of  $1/L$ . The detailed properties of the expansion depend on the ratio  $L/\xi_\pi$ , where  $\xi_\pi = 1/M_\pi$  denotes the Compton wavelength (correlation length) of the Goldstone bosons.

Sizeable finite size effects are expected both for  $\xi_\pi > L$  and for  $\xi_\pi \leq L$ . Then two types of large volume expansion within the chiral perturbation theory at finite volumes can be performed [25, 27, 28]. We shall denote these expansions by the letters  $\mathcal{U}$  and  $\mathcal{V}$  which simultaneously denote the domains of their applicability\*:

\* In the terminology of ref. [26],  $\mathcal{U}$  is the region controlled by the  $\epsilon$ -expansion, while  $\mathcal{V}$  is covered by the  $p$ -expansion.

∥: This domain is characterized by small symmetry breaking. It is the region where the symmetry is restored. Here,

$$M_\pi L \lesssim 1. \tag{3.6}$$

The inequality (3.4) is then satisfied automatically on account of eq. (1.1). The finite size effects are large here. The expansion is in powers of  $L^{-2}$  keeping the total magnetic energy  $u_0$ , eq. (3.3), fixed. Thus  $j$  is treated as a quantity of the order  $O(L^{-4})$ . In ∥ the correlation length  $\xi_\pi$  grows as  $L^2$  for  $L \rightarrow \infty$  [cf. eq. (2.8)].

∇: In this region  $j$  is still small, although larger than in ∥. Finite size effects are smaller than in ∥. It is characterized by

$$M_\pi L \gtrsim 1 \tag{3.7}$$

and, of course, by the inequality (3.4). A typical range observed is  $M_\sigma/M_\pi \gtrsim 5-10$ . Here the symmetry is not restored. The expansion in powers of  $L^{-2}$  in that domain keeps fixed

$$v = \Sigma j L^2 / F^2 = M_\pi^2 L^2. \tag{3.8}$$

For large  $u_0$  the results of the expansion ∥ should smoothly go over into those of the expansion ∇. There is an overlap of the regions of validity of both expansions around  $M_\pi L \approx 1$ ; in our study we find the overlap region to be  $\frac{1}{2} \lesssim M_\pi L \lesssim 1$ . In fig. 1 the dashed line indicates where the ∥- and ∇-regions in the  $\kappa$ - $j$  plane meet for  $L = 10$ .

In subsects. 3.2–3.4 we list those results of expansions ∥ and ∇ which we are going to use in this paper.

### 3.2. FIELD EXPECTATION VALUE FOR SMALL SYMMETRY BREAKING

In the domain ∥ the expectation value of the field  $\langle \varphi_x^0 \rangle_{V,j}$  is given by a series in  $1/L^2$  with coefficients which are non-trivial functions of the product  $jL^4$ . Introducing the quantity

$$u = u_0 \left[ 1 + \frac{3}{2L^2} \frac{\beta_1}{F^2} - \frac{3}{8F^4 L^4} \left\{ \beta_1^2 - 2\beta_2 - \frac{1}{4\pi^2} \ln(\Lambda_M L) \right\} + O(L^{-6}) \right], \tag{3.9}$$

the first two terms in this series may be written in the form [25, 27, 30]

$$\langle \varphi_x^0 \rangle_{V,j} = \frac{u^2 \eta(u)}{jL^4} + 2\rho_2 \frac{\Sigma^2}{F^4} j + O(L^{-6}), \tag{3.10}$$

where

$$\eta(u) = \frac{1}{u} \frac{I_2(u)}{I_1(u)}, \quad (3.11)$$

$$\rho_2 = \frac{3}{4} \left[ \beta_2 + \frac{1}{8\pi^2} \ln(\Lambda_\Sigma L) \right] \quad (3.12)$$

and  $I_1(u)$  and  $I_2(u)$  are the standard modified Bessel functions. The values of the coefficients  $\beta_1$  and  $\beta_2$  depend on the shape of the periodic box. For a symmetric hypercube,  $L_s = L_t$ ,  $\beta_1 = 0.14046$  and  $\beta_2 = -0.0203$ ; values for some other shapes may be found in ref. [30] and in table 3. The finite size scaling formula for the susceptibility conjectured in ref. [29] is a special case of eq. (3.10), obtained by taking the derivative with respect to  $j$  at  $j = 0$ .

Up to corrections  $O(1/L^2)$  the quantity  $u$  is the control parameter  $u_0$ , eq. (3.3), and is thus of order  $O(1)$  in  $\hbar$ . The corrections  $O(L^{-4})$  in (3.9) and (3.10) contain the additional scales  $\Lambda_\Sigma$  and  $\Lambda_M$ . Note that they appear here and in later expressions in logarithmic form only. These correction terms turn out to be very small in the analysis of the data for  $\langle \varphi_x^0 \rangle_{V,j}$  obtained deep in the phase of broken symmetry. Close to the phase transition these terms are not negligible. However, their contribution is too small to allow a reliable determination of the scales even with the available high statistics. We point out that all the observables  $\Sigma$ ,  $F$ ,  $\Lambda_\Sigma$  and  $\Lambda_M$  are quantities defined in infinite volume and for vanishing external source.

In eq. (3.10), the leading term contains the quantity  $u$  rather than  $u_0$ ; strictly speaking, this formula is the result of an expansion at fixed  $u$ . One may of course transform it into an expansion at fixed  $u_0$  by inserting (3.9) and expanding  $\eta(u)$  around  $u_0$  to order  $L^{-4}$ . The difference is however of order  $L^{-6}$  which is beyond the accuracy of this formula and therefore does not have any noticeable consequences in the numerical analysis.

### 3.3. GOLDSTONE CORRELATION FUNCTION FOR SMALL SYMMETRY BREAKING

We denote the correlation function of the fields  $\varphi_x^0$  and  $\varphi_x^i$  by  $G_\sigma$  and  $G_\pi$ ,

$$\langle \varphi_x^0 \varphi_y^0 \rangle_{V,j} = G_\sigma(x-y), \quad (3.13)$$

$$\langle \varphi_x^i \varphi_y^k \rangle_{V,j} = G_\pi(x-y) \delta^{ik}, \quad (3.14)$$

respectively.

For the Goldstone boson component we define the susceptibility

$$a_\pi = \frac{1}{L^4} \sum_{x \in \Lambda} G_\pi(x). \tag{3.15}$$

The O(4) symmetry relates  $a_\pi$  to the expectation value of the field

$$a_\pi = \frac{1}{jL^4} \langle \varphi_x^0 \rangle_{V,j}. \tag{3.16}$$

We analyze the correlation function  $G_\pi(x)$  by integrating over the spatial 3-volume at fixed  $t$ :

$$G_\pi(t) = \frac{1}{L_s^3} \sum_x G_\pi(x, t). \tag{3.17}$$

In the domain  $\ll$  this function can be expanded in powers of  $L^{-2}$  fixing both  $u_0 = \Sigma jL^4$  and  $t/L$ . We analyze the data for  $G_\pi(t)$  on two levels of precision, on which the  $t$ -dependence is determined including the  $O(L^{-2})$  and  $O(L^{-4})$  terms of the expansion  $\ll$ , respectively.

On the  $O(L^{-2})$  level one has

$$G_\pi(t) = a_\pi^0(u) + \frac{L_t^2}{V} b_\pi^0(u) h_1(\tau) + O\left(\frac{1}{L^4}\right), \tag{3.18}$$

where

$$b_\pi^0(u) = \frac{\Sigma^2}{F^2} [1 - \eta(u)], \tag{3.19}$$

$$\tau = t/L_t. \tag{3.20}$$

Eqs. (3.16) and (3.10) give

$$a_\pi^0(u) = \frac{u^2 \eta(u)}{(jL^4)^2}. \tag{3.21}$$

For consistency, we use here  $u = u_0(1 + 3\beta_1/2F^2L^2)$  when working at the  $O(L^{-2})$  level.

On the  $O(L^{-4})$  level the integrated propagator (3.17) has the form

$$G_{\pi}(t) = a_{\pi}(u) + \frac{L_t^2}{V} b_{\pi}(u) h_1(\tau) + \left( \frac{L_t^2}{V} \right)^2 [c_{\pi}(u) h_2(\tau) + d_{\pi}(u) h_3(\tau)] + \frac{1}{V} e_{\pi} [\delta(\tau) - 1] + O\left(\frac{1}{L^6}\right). \quad (3.22)$$

In the large volume expansion at fixed  $t/L$  short range contributions such as those of the form  $G(t) \propto L^{-3} \exp(-M_{\sigma} t)$  generated by the exchange of a  $\sigma$ -particle manifest themselves only at order  $L^{-4}$  through the term  $e_{\pi} \delta(\tau)$ . In the region  $t \gg M_{\sigma}^{-1}$ , this term does not contribute – the  $t$ -dependence of the propagator is governed by the exchange of Goldstone bosons. At order  $L^{-2}$ , only single particle exchange contributes, giving rise to a parabolic time dependence. The exchange of two Goldstone bosons manifests itself at order  $L^{-4}$ , through the functions  $h_2(\tau)$  and  $h_3(\tau)$ . At the accuracy we are considering here, the coefficients of the time dependent contributions involve the constants  $F$  and  $\Sigma$  only,

$$a_{\pi}(u) = a_{\pi}^0(u) + \frac{2\rho_2 \Sigma^2}{F^4 V}, \quad (3.23)$$

$$b_{\pi}(u) = b_{\pi}^0(u) \left( 1 + \frac{\beta_1}{L^2 F^2} \right) + O(L^{-4}), \quad (3.24)$$

$$c_{\pi}(u) = \frac{\Sigma^2}{F^4} [1 + (2 + u^2) \eta(u)] + O(L^{-2}), \quad (3.25)$$

$$d_{\pi}(u) = \frac{3}{2} \frac{\Sigma^2}{F^4} \eta(u) + O(L^{-2}), \quad (3.26)$$

but the constant term ( $a_{\pi} - e_{\pi}/V$ ) receives the contribution of order  $L^{-4}$  from the logarithmic scales  $\Lambda_{\Sigma}, \Lambda_F, \Lambda_M$  (for the explicit expression, see ref. [30]). However, since our data analysis concentrates on the  $t$ -dependence of  $G_{\pi}(t)$ , we do not need the constant term to this accuracy here.

The functions  $h_i(\tau)$ ,  $i = 1, 2, 3$ , arise from the spatial integral over the propagator associated with the non-zero momentum modes. On the interval  $0 < t < L_t$  they

are given by

$$h_1(\tau) = \frac{1}{2} \left[ \left( \frac{1}{2} - \tau \right)^2 - \frac{1}{12} \right], \quad (3.27)$$

$$h_2(\tau) = \frac{1}{24} \left[ \tau^2 (1 - \tau)^2 - \frac{1}{30} \right], \quad (3.28)$$

$$h_3(\tau) = [h_1(\tau)]^2 + \sum_{n \neq 0} \left\{ \frac{\cosh[q_n(\frac{1}{2} - \tau)]}{2q_n \sinh q_n/2} \right\}^2, \quad (\tau > 0) \quad (3.29)$$

where  $n = (n_1, n_2, n_3)$  are integers which do not vanish simultaneously and

$$q_n = 2\pi \frac{L_t}{L_s} |n|. \quad (3.30)$$

At  $\tau = 0$ ,  $h_3(0)$  is defined [30] such that the integral of  $h_3(\tau)$  over the interval  $0 \leq \tau \leq 1$  vanishes, as it does for  $h_1$  and  $h_2$ .

For large volumes and small sources, the correlation function  $G_\pi(\tau)$  must show a parabolic time dependence generated in leading order chiral perturbation theory by a one-Goldstone exchange. The contributions of  $O(1/L^4)$  to the correlation functions have been calculated by evaluating the chiral perturbation series to the next order [30]. These Goldstone pair contributions are controlled by the same two constants  $\Sigma, F$  which determine the leading terms. They consist of

- (i) short-range contributions represented by a  $\delta$ -function at  $t = 0 \pmod{L_t}$ ,
- (ii) non-parabolic terms generated by the exchange of a pair of Goldstone bosons,
- (iii) a change of the coefficient  $a_\pi$  which turned out to be unimportant numerically, and
- (iv) a change from  $b_\pi^0$  to  $b_\pi$ , which plays an important role in the data analysis.

#### 3.4. FIELD EXPECTATION VALUE BEYOND THE SYMMETRY RESTORATION DOMAIN

In the domain  $\mathcal{V}$  one should switch to the  $1/L^2$  expansion at fixed  $t$ , eq. (3.8). One may write this expansion in powers of  $M_\pi^2$ , eq. (2.8), as from (3.8) we have  $j \propto 1/L^2$ . For the scalar field expectation value one gets [25]

$$\langle \varphi_x^0 \rangle_{\mathcal{V}, j} = \Sigma \left( 1 - \frac{3}{2F^2} g_1(M_\pi) - \frac{3}{16\pi^2 F^2} M_\pi^2 \ln \frac{M_\pi}{\Lambda_s} + O(M_\pi^4) \right), \quad (3.31)$$

where

$$g_1(M) = \frac{1}{16\pi^2} \int_0^\infty \frac{d\lambda}{\lambda^2} \exp(-\lambda M^2) \sum_{\underline{n} \neq 0} \exp\left(-\frac{a_{\underline{n}}^2}{4\lambda}\right), \quad (3.32)$$

$$a_{\underline{n}} = (L_s n_1, L_s n_2, L_s n_3, L_t n_4). \quad (3.33)$$

Formula (3.31) can be used for extracting from the data a value for the parameter  $\ln \Lambda_\Sigma$ . That parameter, in turn, can be related to  $M_\sigma$  by means of renormalized perturbation theory [31,39]. For the renormalized mass  $M_R$  in the renormalization scheme of ref. [31] (appendix B) one finds from a one loop calculation

$$\ln M_R = \ln \Lambda_\Sigma + \frac{7}{6} - \frac{16\pi^2}{3} \frac{F^2}{M_R^2} = \ln \Lambda_M + \frac{7}{3} - 16\pi^2 \frac{F^2}{M_R^2}. \quad (3.34)$$

The physical mass  $M_\sigma$  is connected with  $M_R$  by a one loop order calculation

$$M_\sigma^2 = M_R^2 \left[ 1 + \frac{M_\sigma^2}{2F^2} \frac{1}{16\pi^2} (3\pi\sqrt{3} - 13) \right]. \quad (3.35)$$

The value of  $M_\sigma$  differs from  $M_R$  only by a few percent in the perturbative region.

#### 4. Discussion of the numerical data

Most of our data for the model (2.3) have been obtained for  $J > 0$ . Using a 2-hit standard Metropolis algorithm we have worked on the lattices  $L_s^3 L_t$  with periodic boundary conditions, mainly on symmetric lattices but sometimes also with  $L_t > L_s$ . Sampling the path integral at small external field  $J$  requires high statistics. We typically accumulated  $(0.3-1) \times 10^6$  Metropolis sweeps on all lattices. Our data points with the corresponding values of the parameters  $\kappa$ ,  $J$ ,  $L_s$  and  $L_t$ , are listed in table 1.

The data for  $J > 0$  have been obtained at 5 values of the hopping parameter:  $\kappa = 0.355, 0.330, 0.325, 0.310$  and  $0.3075$ , all in the broken phase. Since the restriction (1.1) appears to be crucial we give in table 2 approximate values for  $M_\sigma$  obtained in our earlier [9,11,12] and recent [40] calculations for  $J = 0$  at these  $\kappa$ -points. It is apparent that for the three larger values of  $\kappa$  the mass  $M_\sigma$  is sufficiently large so that the chiral perturbation theory can be reliably tested on

TABLE 1

List of the data points with indicated domain  $\mathcal{W}/\mathcal{V}$ , statistics in megasweeps  $Msw$  and the ratio  $A$ , eq. (4.1). We give for each data point the values of  $\langle \varphi_x^0 \rangle_{V,j}$  and  $\Sigma$  determined by means of eq. (3.10) up to order  $1/L^2$ . In most cases where the expansion  $\mathcal{W}$  is applicable the coefficients  $a_\pi$  and  $b_\pi$  determining the first line in the expression (3.22) for the Goldstone correlation function are given

$\kappa$ $\mathcal{W}/\mathcal{V}$	$J$ $j$	$L_s$ $L_t$	$Msw$ $A$	$\langle \varphi_x^0 \rangle_{V,j}$ $\Sigma$	$a_\pi$ $b_\pi$
0.355	0.012	8	0.3	0.38871(81)	-
$\mathcal{V}$	0.0142	8	1.050(48)	-	-
0.355	0.008	8	0.3	0.3771(11)	-
$\mathcal{V}$	0.00949	8	0.945(52)	-	-
0.355	0.005	8	0.5	0.3518(19)	0.351(21)
$\mathcal{W}$	0.00593	8	0.998(50)	0.4036(19)	0.8941(73)
0.355	0.004	8	0.3	0.3322(48)	0.350(49)
$\mathcal{W}$	0.00475	8	1.06(12)	0.3983(50)	0.874(10)
0.355	0.003	8	0.5	0.3112(46)	0.316(28)
$\mathcal{W}$	0.00356	8	1.017(81)	0.4005(48)	0.8500(78)
0.355	0.0029	8	0.84	0.3085(39)	0.314(21)
$\mathcal{W}$	0.00344	8	1.019(62)	0.4010(40)	0.8505(50)
0.355	0.002	8	0.501	0.2650(64)	0.277(25)
$\mathcal{W}$	0.00237	8	1.045(94)	0.3970(69)	0.8181(89)
0.355	0.0015	8	1.	0.2165(81)	0.243(11)
$\mathcal{W}$	0.00178	8	1.124(82)	0.3835(94)	0.7902(49)
0.355	0.00125	8	1.6	0.2132(84)	0.202(11)
$\mathcal{W}$	0.00148	8	0.949(76)	0.409(10)	0.7872(50)
0.355	0.001	8	1.	0.1821(96)	0.174(17)
$\mathcal{W}$	0.00119	8	0.96(11)	0.408(12)	0.7708(91)
0.355	0.0008	8	0.8	0.133(13)	0.1495(90)
$\mathcal{W}$	0.000949	8	1.12(16)	0.378(22)	0.7599(63)
0.355	0.0005	8	0.5	0.086(16)	-
$\mathcal{W}$	0.000593	8	-	0.374(39)	-
0.355	0.002	10	0.5	0.3448(33)	0.353(64)
$\mathcal{W}$	0.00237	10	1.023(90)	0.4009(34)	0.888(10)
0.355	0.0018	10	0.6	0.3379(33)	0.343(75)
$\mathcal{W}$	0.00214	10	1.02(10)	0.4004(34)	0.8768(91)
0.355	0.0016	10	1.5	0.3361(20)	0.315(35)
$\mathcal{W}$	0.00190	10	0.937(50)	0.4069(20)	0.8615(48)
0.355	0.0012	10	1.5	0.3130(38)	0.289(43)
$\mathcal{W}$	0.00142	10	0.924(70)	0.4076(39)	0.8547(61)
0.355	0.0014	10	0.8	0.3189(42)	0.325(44)
$\mathcal{W}$	0.00166	10	1.020(73)	0.3999(42)	0.8484(81)
0.355	0.00075	10	0.4	0.263(10)	0.237(37)
$\mathcal{W}$	0.000890	10	0.901(96)	0.410(11)	0.8161(75)
0.355	0.002	12	0.3	0.3771(18)	0.36(13)
$\mathcal{W}$	0.00237	12	0.95(10)	0.4036(18)	0.917(13)
0.355	0.001	12	0.3	0.3523(38)	0.31(11)
$\mathcal{W}$	0.00119	12	0.88(10)	0.4080(38)	0.885(12)
0.355	0.0007	12	0.3	0.3210(86)	0.32(21)
$\mathcal{W}$	0.000831	12	0.99(21)	0.4007(88)	0.874(19)
0.355	0.0004	12	0.3	0.255(15)	0.25(13)
$\mathcal{W}$	0.000475	12	1.00(20)	0.389(17)	0.799(20)
0.355	0.0003	12	0.3	0.237(17)	0.22(13)
$\mathcal{W}$	0.000356	12	0.93(23)	0.409(19)	0.792(26)

(continued)

$\kappa$ // $\gamma$	$J$ $j$	$L_s$ $L_t$	Msw $A$	$\langle \varphi_x^0 \rangle_{V,j}$ $\Sigma$	$a_\pi$ $b_\pi$
0.33	0.007	8	0.5	0.27762(94)	-
$\gamma$	0.00862	8	1.151(52)	-	-
0.33	0.006	8	0.5	0.2693(14)	-
$\gamma$	0.00739	8	1.178(53)	-	-
0.33	0.005	8	0.5	0.2579(18)	-
$\gamma$	0.00615	8	-	-	-
0.33	0.004	8	0.5	0.2442(26)	-
$\gamma$	0.00492	8	-	-	-
0.33	0.003	8	0.5	0.2238(32)	-
//	0.00369	8	-	0.3054(34)	-
0.33	0.002	8	0.5	0.1860(58)	0.1506(68)
//	0.00246	8	0.811(52)	0.3055(66)	0.8416(25)
0.33	0.002	10	0.8	0.2503(20)	0.253(34)
//	0.00246	10	1.014(66)	0.3019(21)	0.8812(73)
0.33	0.0016	10	1.1	0.2377(25)	0.233(39)
//	0.00197	10	0.981(80)	0.3031(26)	0.879(10)
0.33	0.0012	10	1.2	0.2117(32)	0.231(40)
//	0.00148	10	1.092(99)	0.2987(34)	0.837(14)
0.33	0.0008	10	1.2	0.1634(59)	0.184(28)
//	0.000985	10	1.13(11)	0.2865(68)	0.797(15)
0.33	0.14	12	0.42	0.3985(12)	-
$\gamma$	0.172	12	1.009(11)	-	-
0.33	0.12	12	0.42	0.3900(13)	-
$\gamma$	0.148	12	0.994(11)	-	-
0.33	0.1	12	0.42	0.3805(14)	-
$\gamma$	0.123	12	0.998(11)	-	-
0.33	0.08	12	0.076	0.3698(37)	-
$\gamma$	0.0985	12	0.996(27)	-	-
0.33	0.06	12	0.42	0.3577(18)	-
$\gamma$	0.0739	12	0.998(14)	-	-
0.33	0.02	12	0.42	0.3247(30)	-
$\gamma$	0.0246	12	0.984(24)	-	-
0.33	0.018	12	0.42	0.3224(32)	-
$\gamma$	0.0222	12	0.977(24)	-	-
0.33	0.008	12	0.42	0.3074(48)	-
$\gamma$	0.00985	12	1.059(41)	-	-
0.33	0.004	12	0.42	0.2956(65)	-
$\gamma$	0.00492	12	1.002(50)	-	-
0.33	0.002	12	0.92	0.27953(77)	-
$\gamma$	0.00246	12	0.977(26)	-	-
0.33	0.0015	12	0.92	0.2694(10)	0.265(23)
//	0.00185	12	0.986(28)	0.3027(10)	0.9076(44)
0.33	0.001	12	0.92	0.2528(16)	0.239(21)
//	0.00123	12	0.948(30)	0.3046(17)	0.8733(61)
0.33	0.0005	12	0.92	0.1923(38)	0.207(15)
//	0.000615	12	1.076(44)	0.2937(41)	0.8031(90)
0.33	0.0001	12	0.42	0.073(20)	0.0567(36)
//	0.00123	12	0.78(23)	0.339(50)	0.739(10)
0.325	0.008	8	0.84	0.25981(67)	-
$\gamma$	0.00992	8	1.038(18)	-	-

(continued)

$\kappa$ // $\gamma$	$J$ $j$	$L_s$ $L_t$	Msw $A$	$\langle \varphi_x^0 \rangle_{V,j}$ $\Sigma$	$a_\pi$ $b_\pi$
0.325	0.004	8	0.84	0.2229(14)	-
$\gamma$	0.00496	8	0.994(22)	-	-
0.325	0.002	8	0.84	0.1618(40)	0.1615(39)
//	0.00248	8	1.000(42)	0.2768(47)	0.8317(31)
0.325	0.001	8	0.84	0.0956(62)	0.0981(17)
//	0.00124	8	1.027(80)	0.274(10)	0.8029(28)
0.325	0.0007	8	0.84	0.0764(63)	0.0706(13)
//	0.000868	8	0.925(89)	0.289(13)	7949(30)
0.325	0.008	10	0.84	0.27850(29)	-
$\gamma$	0.00992	10	0.986(17)	-	-
0.325	0.004	10	0.64	0.25893(76)	-
$\gamma$	0.00496	10	0.971(25)	-	-
0.325	0.002	10	0.64	0.2248(24)	0.231(17)
//	0.00248	10	1.029(44)	0.2750(24)	0.8689(82)
0.325	0.0007	10	0.84	0.1364(61)	0.1449(79)
//	0.000868	10	1.064(73)	0.2685(76)	0.788(10)
0.325	0.001	10	0.64	0.1850(37)	0.168(10)
//	0.00124	10	0.907(43)	0.2863(40)	0.837(10)
0.325	0.004	12	0.96	0.27130(29)	-
$\gamma$	0.00496	12	0.984(20)	-	-
0.325	0.002	12	0.96	0.25377(71)	-
$\gamma$	0.00248	12	0.997(25)	-	-
0.325	0.001	12	0.96	0.2220(19)	0.229(20)
//	0.00124	12	1.034(34)	0.2725(19)	0.873(12)
0.325	0.0007	12	0.96	0.2048(23)	0.196(16)
//	0.000868	12	0.959(33)	0.2775(24)	0.843(14)
0.325	0.0005	12	0.96	0.2114(47)	0.184(23)
//	0.000620	16	0.87(11)	0.2891(48)	0.848(16)
0.325	0.0003	12	0.96	0.1778(97)	0.136(18)
//	0.000372	16	0.76(13)	0.301(10)	0.800(22)
0.325	0.0002	12	0.96	0.119(11)	0.120(10)
//	0.000248	16	1.01(18)	0.277(16)	0.740(19)
0.31	0.001	8	0.96	0.0747(29)	0.0691(26)
//	0.00127	16	0.93(14)	0.1727(42)	0.83(23)
0.31	0.0005	8	0.96	0.0314(41)	0.0379(11)
//	0.000635	16	1.21(26)	0.148(11)	0.83(19)
0.31	0.001	10	0.96	0.1010(42)	0.1073(96)
//	0.00127	16	1.07(19)	0.1576(48)	0.85(83)
0.31	0.0005	10	0.96	0.0662(45)	0.0665(33)
//	0.000635	16	1.01(14)	0.1622(69)	0.82(57)
0.3075	0.001	8	0.96	0.0506(27)	0.0536(19)
//	0.00128	16	1.06(17)	0.1351(45)	0.88(16)
0.3075	0.0005	8	0.96	0.0273(32)	0.02825(99)
//	0.000638	16	1.04(23)	0.1361(96)	0.85(17)
0.3075	0.001	10	0.96	0.0820(22)	-
$\gamma$	0.00128	16	0.98(11)	-	-
0.3075	0.0005	10	0.96	0.0441(35)	0.0481(18)
//	0.000638	16	1.09(15)	0.1254(64)	0.87(31)

TABLE 2  
 Infinite volume quantities  $\Sigma$ ,  $\langle |\overline{\varphi^a}| \rangle$ ,  $F$ ,  $Z$ ,  $M_\sigma$  and  $g_R = M_\sigma^2/2F^2$

$\kappa$	$\Sigma$	$\langle  \overline{\varphi^a}  \rangle$	$F$	$Z$	$M_\sigma$	$g_R$
0.355	0.40361(86)	0.402	0.4109(12)	0.965(2)	1.09(10)	3.52(70)
0.330	0.3027(11)	0.301	0.3075(16)	0.969(3)	0.92(7)	4.47(62)
0.325	0.2769(12)	0.276	0.2807(19)	0.973(5)	0.81(2)	4.16(26)
0.310	0.1643(63)	0.163	0.1668(71)	0.97(1)	0.39(2)	2.73(51)
0.3075	0.132(13)	0.128	0.135(14)	0.96(1)	0.29(1)	2.31(63)

The error of  $\Sigma$  includes a possible systematic error coming from  $1/L^4$  corrections within the framework of the  $\llcorner$  expansion.  $\langle |\overline{\varphi^a}| \rangle$  has been calculated from the scaling law fit in ref. [12], we omit errors as  $1/L^4$  corrections were not considered there. The wave function renormalization at  $\kappa = 0.355$ , 0.330 and 0.325 has been calculated in this paper, while the values at 0.310 and 0.3075 are from our earlier work. The scalar mass results from a  $1/L^2$  infinite volume extrapolation of the finite volume propagator mass and a subsequent scaling law fit as described in ref. [12].

lattices of available sizes  $L = 8-16$ . The two lower  $\kappa$ -points lie in the region where one would like to estimate the upper bound on the Higgs boson mass, corresponding in the  $\Phi^4$  theory to an upper bound on  $M_\sigma$ , i.e.  $\xi_\sigma \approx 2-3$ . Here some deviations from chiral perturbation theory can be expected for small lattices. Of course, the onset and the form of these deviations are themselves of interest for future applications of chiral perturbation theory, e.g. within QCD calculations, so we want to identify them.

The choice of the values of  $J$  and of the lattice size has been made with regard to the requirements (3.4), (3.6) and (3.7). Using (2.8) and the mean field scaling laws for  $M_\sigma$  and  $\Sigma$  (both quantities scale up to logarithmic corrections as  $\sqrt{\kappa - \kappa_c}$ , with coefficients known from numerical simulations) one can determine, for a given  $L$ , the domains  $\llcorner$  and  $\lrcorner$  in the  $\kappa$ - $j$  plane (see fig. 1), where the chiral perturbation expansions are expected to be valid.

The problem of correlations between the configurations in Monte Carlo runs was taken into account by the blocking method for the error analysis. It consists of blocking the data into bunches of different length, ranging from 0.5-40 kilosweeps. On each block the fit for the quantity of interest has been performed and the block values for this quantity evaluated. These blocked data give then the average value and the error of the corresponding quantity. We found a clear dependence of the error on the length of the bunches. For  $J$ -values at the order of 0.001 we found the error to be stable with a block length of 2 ksweeps. For smaller values of  $J$  and close to the phase transition the minimal block length to reach a stable error plateau was found to be 16 ksweeps. This detailed error analysis was done, however, only for a subset of the data points and, based on these results, we have scaled the naive errors at other data points accordingly.

A check on the data and errors provided by the identity (3.16) is non-trivial: the calculation of  $a_\pi$  requires good quality data for the correlation function (3.14) at large distances. We have included in table 1 the ratio

$$A = \frac{jL^4 a_\pi}{\langle \varphi_x^0 \rangle_{V,j}} \quad (4.1)$$

with  $\langle \varphi_x^0 \rangle_{V,j}$  measured directly and  $a_\pi$  determined from the Goldstone boson correlation function by means of eq. (3.15). We found that for most of the data points the ratio  $A$  is consistent with 1 within the error bars. A few data points with  $A$  significantly different from 1 have been excluded from the analysis (it is amusing to mention that in this way we have even detected an inconspicuous hardware error which occurred during one of our runs).

We have measured  $\langle \varphi_x^0 \rangle_{V,j}$  and  $G_\pi(t)$  for  $t = 0, \dots, L_t/2$  at all data points. A file with these raw data is available from the authors on request. In table 1 we give the values of  $\langle \varphi_x^0 \rangle_{V,j}$  and of the coefficients  $a_\pi, b_\pi$  obtained from the analysis of  $G_\pi(t)$  by means of eq. (3.22) at each data point. The coefficient  $b_\pi$  provides a quite complete information about the  $t$ -dependence of  $G_\pi(t)$  for each data point. The other relevant terms in eq. (3.22) give only a small contribution and can be calculated from eqs. (3.25) and (3.26) using the values of  $\Sigma$  and  $F$  obtained from the data analysis and listed in table 2.

Approaching the critical point, critical slowing down decreases the effectiveness of the Metropolis Monte Carlo process. This difficulty has been overcome recently by the development of non-local, so-called cluster algorithms [37]. Most of our data for  $j \neq 0$  have been obtained previous to the introduction of this method. With the new algorithm we have obtained some data for  $J = 0$  on lattices of ‘‘cylinder’’ geometry,  $L_t \gg L_s$ . These data points are listed in table 3. Even for  $L_t$  as large as 80 we had no problems: thermalization has been easily achieved within 50 kilosweeps. It is in the cylinder geometry where the power of the cluster algorithms is most striking [38]. We have also accumulated some data for  $j = 0$  at  $\kappa = 0.355$  and 0.33 for a range of lattices  $4^4$ – $16^4$ .

Although we have the corresponding data we do not deal with  $G_\sigma(x)$ , eq. (3.13), here. The reason is that the contribution of the  $\sigma$ -particle to the propagators, which is obviously more important in  $G_\sigma(x)$  than in  $G_\pi(x)$ , is not properly taken into account by chiral perturbation theory. Therefore the condition (3.5) has to be fulfilled very stringently, which usually leaves only a few data points for  $G_\sigma$  at large  $t$ . We have checked that these data are consistent with the chiral expansion; for a reliable extraction of the low energy constants they are insufficient, however. A complete analysis of  $G_\sigma(x)$ , which could also provide valuable information about  $M_\sigma$ , requires some ingredients beyond chiral perturbation theory and will be attempted in a separate work.

TABLE 3  
 Values of  $F$  as obtained from the  $O(4)$  symmetric propagator (subject. 6.2).  
 The second column gives the spatial and the third column the  
 time extent of the lattice

$\kappa$	$L_s$	$L_t$	$\beta_1$	$F_L$	$F_{\text{cyl}}$	$F$
0.310	8	32	0.143	0.179(1)	0.156(1)	0.167(7)
0.310	8	40	0.285	0.178(1)	0.155(1)	"
0.310	8	120	2.640	0.178(1)	0.155(1)	"
0.310	10	32	0.048	0.171(1)	0.157(1)	"
0.310	10	40	0.143	0.169(1)	0.154(1)	"
0.310	12	32	-0.004	0.168(2)	0.158(1)	"
0.310	14	32	-0.035	0.164(2)	0.157(1)	"
0.310	14	80	0.399	0.166(2)	0.159(1)	"
0.320	8	40	0.285	0.261(1)	0.247(1)	0.249(4)
0.320	10	40	0.143	0.257(2)	0.248(1)	"
0.355	8	40	0.285	0.418(10)	0.409(5)	0.411(1)
0.355	10	40	0.143	0.420(1)	0.415(1)	"
0.355	10	80	0.831	0.418(11)	0.413(6)	"

$\beta_1$  is the corresponding shape coefficient. The quantity  $F_L$  denotes the value of  $F$  calculated by means of the zeroth order of the relations (6.5) and (6.6) whereas  $F_{\text{cyl}}$  is calculated including first order corrections there. For comparison we give in the last column the values of  $F$  obtained from the expansion  $\not\sim$  (see also table 2). For  $\kappa = 0.32$ ,  $F^2$  is interpolated linearly from the values at  $\kappa = 0.31$  and  $\kappa = 0.325$ . Note the strong dependence of  $F_L$  on the lattice size, whereas  $F_{\text{cyl}}$  is nearly constant and in good agreement with  $F$  from the expansion  $\not\sim$ .

## 5. Results for non-vanishing external source

### 5.1. FIELD EXPECTATION VALUE

The results for  $\langle \varphi_x^0 \rangle_{V,j}$  are displayed in fig. 2. The data at the lower values of  $j$ , where the full curves are drawn, belong to the domain  $\not\sim$ . As expected, they are  $j$ -dependent and show very strong finite size effects, in particular in the vicinity of  $j = 0$ . The challenge is to describe these very different results for each  $\kappa$  by means of eq. (3.10) (the expansion  $\not\sim$ ) in terms of only two parameters,  $\Sigma$  and  $F$ .

Fitting all the data for  $\langle \varphi_x^0 \rangle_{V,j}$  in the domain  $\not\sim$  one can determine both  $\Sigma$  (from the leading term in eqs. (3.10) and (3.9)) and, in principle, also  $F$  (from the non-leading correction  $O(1/L^2)$  in eqs. (3.10) and (3.9)). For our fit we consider only the terms up to  $O(L^{-2})$  of these equations; a fit including the higher order terms serves as a method to estimate the systematic uncertainty. The fit determines  $\Sigma$  reliably with a very small error. The values of  $F$  obtained in a preliminary analysis had a large error, however. We could only conclude that the values of  $Z$  calculated from  $F$  by means of eq. (2.7) were within their large error bars

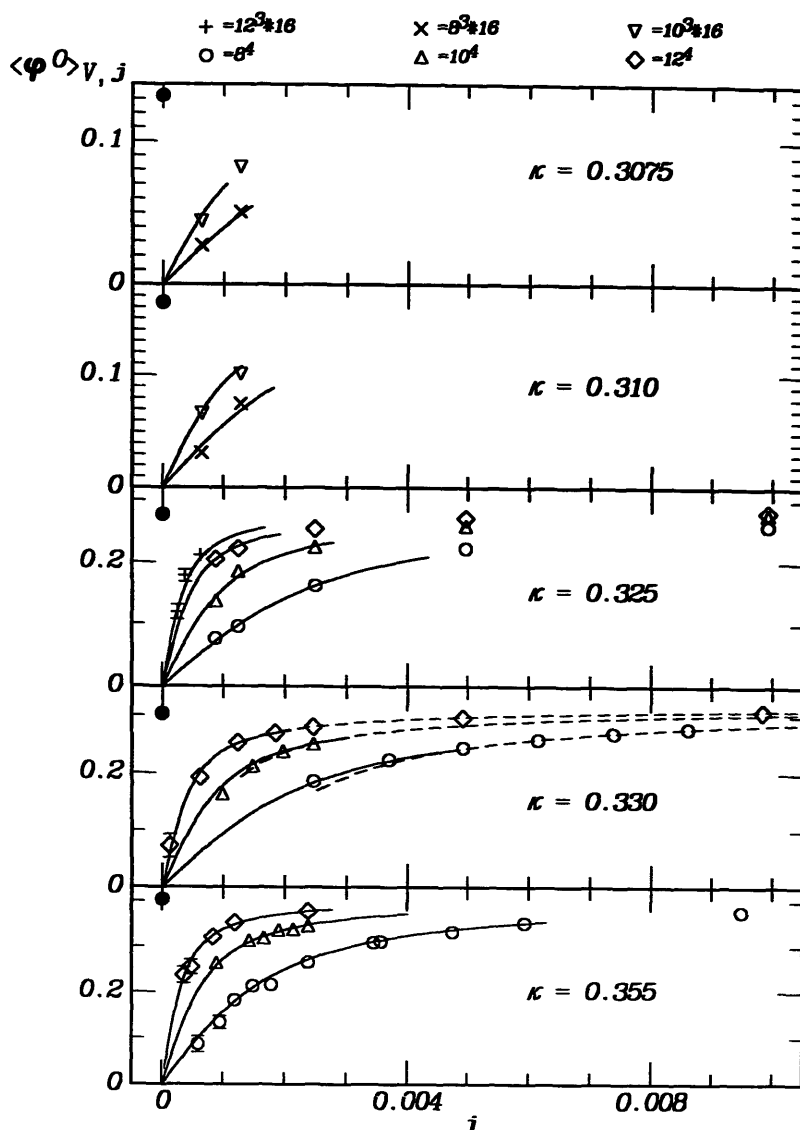


Fig. 2. Expectation values  $\langle \varphi_x^0 \rangle_{V,j}$  on lattices of various sizes at the considered values of  $\kappa$ . The solid curves correspond to fits by means of the expansion  $\mathcal{H}$ , eq. (3.10), up to order  $1/L^2$ . They are drawn only in the region where the  $\mathcal{H}$ -expansion according to eq. (3.6) is valid. The solid circles in the upper-left corners of the graphs mark the fitted values of  $\Sigma$  which are given in table 2. The dashed curves at  $\kappa = 0.33$  correspond to a fit by means of the expansion  $\mathcal{H}'$ , eq. (3.31) in the domain (3.6). If the error bars here and in the following figures are not shown they are smaller than the symbol sizes.

consistent with a number around 1. As the non-leading term in eq. (3.9) contributes only a few %, it is difficult to determine  $F$  even from very precise data for  $\langle \varphi_x^0 \rangle_{V,j}$ . As will be explained in subsect. 5.2, the Goldstone boson propagator is much more suitable for this purpose.

It is known already from our previous calculations, both at  $j = 0$  [9, 11] and  $j > 0$  [12, 32], as well as from the results of other groups [8, 10], that in the considered  $\kappa$ -range  $Z$  is about 0.98. This is confirmed also by our analysis of  $G_\pi(t)$  in sect. 6.

Therefore in the further analysis of  $\langle \varphi_x^0 \rangle_{V,j}$  we have taken  $Z = 1$  and thus set  $F = \Sigma$  in eq. (3.9) and determined only  $\Sigma$ . We have also checked that the results for  $\Sigma$  do not change if the value  $Z = 0.98$  is assumed.

At each  $\kappa$  we did a simultaneous fit using the expression (3.10) to all the data at various  $j$  and  $L$  in  $\mathcal{A}$ . The full curves in fig. 2 give the results of this fit. The values for  $\Sigma$  obtained in this way are shown in fig. 2, too (large dots in the upper left corners). It is remarkable how much the measured values of  $\langle \varphi_x^0 \rangle_{V,j}$  differ from the final numbers for  $\Sigma$ . Nevertheless, all these data agree precisely with the full curves (3.10) with  $\Sigma$  obtained from the joint fit. The figure also demonstrates how dangerous an attempt could be to try to obtain the correct value of  $\Sigma$  by means of some linear (or any other) extrapolation of  $\langle \varphi_x^0 \rangle_{V,j}$  to  $j = 0$ .

Alternatively one may invert (3.10) individually for each  $\langle \varphi_x^0 \rangle_{V,j}$  in  $\mathcal{A}$ . The results for  $\Sigma$  (listed in table 1) are consistent with the value of  $\Sigma$  from the joint fit at the corresponding  $\kappa$ , though some scattering of the data can be observed. Thus, chiral perturbation theory allows us to determine the quantity  $\Sigma$  for infinite volume and zero external source from the measured field expectation value at *one* suitably chosen value of the external source  $j$  on a lattice of *one* suitable size.

The power of this method has been already observed in our earlier work [11, 12] at a rather large distance from the critical point, for  $\kappa = 0.355, 0.330$  and  $0.325$  on hypercubic lattices,  $L_t = L_s$ . We give these data here for completeness. We have now verified at  $\kappa = 0.325$  on the  $12^3 \times 16$  lattice that the method also works on asymmetric lattices. In this work we also include the points  $\kappa = 0.310$  and  $0.3075$ , which are of physical interest and where the condition (1.1) is satisfied with a smaller security margin than at the points we have studied earlier. Here we find first indications of systematic errors. They may be estimated by performing the analysis based on eq. (3.9) considering terms up to  $O(1)$ ,  $O(L^{-2})$ , and  $O(L^{-4})$ , respectively. We find remarkably fast convergence at larger  $\kappa$ . The corresponding values for  $\Sigma$  at  $\kappa = 0.355$  are  $0.40923, 0.40361$  and  $0.40354$ . Closer to the phase transition the results indicate larger systematic uncertainties, i.e. for  $\Sigma$  at  $\kappa = 0.310$  we obtain values  $0.17526, 0.16439$  and  $0.15808$ . Thus at the smaller values of  $\kappa$  we expect systematic errors up to 4%. We include these estimates of the systematic errors in the errors given in table 2.

To summarize: The expansion describes the data satisfactorily throughout the domain of  $\kappa$  considered here. As seen in fig. 2, even the points at larger values of  $j$ , which are outside the domain  $\mathcal{A}$ , tend to lie on the continuation of the curves (3.10). However, at values of  $\kappa$  close to the critical point we notice an increase of the systematic error if one neglects higher order terms.

The results for  $\Sigma$  are listed in table 2 and  $\Sigma^2$  is shown in fig. 3 as a function of  $\kappa$ . The values lie on the scaling law line

$$\Sigma^2 = C_\Sigma^2 \left( \frac{\kappa - \kappa_c}{\kappa_c} \right) \ln^{1/2} \left( \frac{\kappa - \kappa_c}{\kappa_c} \right). \quad (5.1)$$

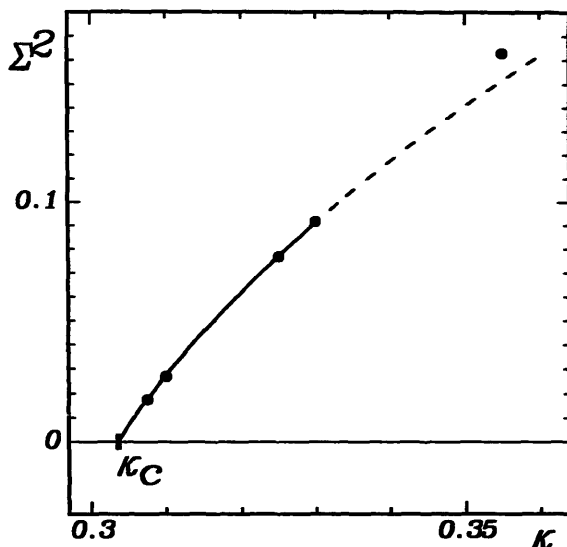


Fig. 3. Scaling law fit according to eq. (5.1) to the infinite volume  $\Sigma$ -values. Only the points  $\kappa \leq 0.33$  have been used for the fit (solid line). The error of  $\kappa_c$  is indicated on the  $\Sigma = 0$  axis.

A deviation from the leading linear behaviour is observable and compatible with the logarithmic correction. Imposing the formula (5.1) to the results for  $\Sigma$  we obtain from the fit

$$\kappa_c = 0.3036(10), \quad C_\Sigma^2 = 0.672(6). \tag{5.2}$$

The value of  $\kappa_c$  is in agreement with  $\kappa_c = 0.3045(7)$  obtained in our earlier calculations [11] at  $j = 0$  using the approximation (3.2). Here the error on  $\kappa_c$  includes the systematic error induced by the  $O(L^{-4})$  corrections. If one includes an estimation of these corrections as described above,  $\kappa_c$  is shifted to a value of  $\kappa_c = 0.3046$ . The results (5.2) are also in good agreement with those of other authors [8, 10].

In table 2 we also include the values for  $\Sigma$  obtained in our previous calculations at  $j = 0$  [9, 11] by means of the approximation (3.2). The excellent agreement demonstrates that systematic errors of the method (3.2) used at  $j = 0$  are remarkably small.

We now turn to the data for  $\langle \varphi_x^0 \rangle_{V,j}$  obtained at larger values of  $j$  in the domain  $\mathcal{V}$ . They ought to be analyzed according to eq. (3.31) and indeed this equation describes the data nicely. This provides us with the possibility to determine the scale parameter  $\Lambda_\Sigma$ . We fix the value of  $\Sigma$  to that obtained from the analysis in the domain  $\mathcal{V}$  and fit the data accordingly. The resulting curves are exhibited in fig. 2 (dashed lines for  $\kappa = 0.330$ ) and are in excellent agreement with the data. One notices a sizeable overlap with the data at small  $j$  in the domain  $\mathcal{V}$ .

The fit provides an estimate for  $\ln \Lambda_\Sigma$  at  $\kappa = 0.33$ ,  $\ln \Lambda_\Sigma = 3.3(4)$ . With the perturbative relations (3.34) and (3.35) of this parameter to  $M_\sigma$  [31, 39] we obtain

$M_\sigma = 1.06(8)$ . Here we regard however the fitted value for  $\ln \Lambda_\Sigma$  as rather imprecise, especially as slight modifications of the fit procedure, like omitting or including data points, leads to a larger scattering of the fitted values than indicated by the quoted statistical error alone. The value obtained is smaller than the one obtained by an alternative determination of  $\Lambda_\Sigma$  described below. Still, this indirect determination of  $M_\sigma$  agrees remarkably well with the value obtained from the propagator,  $M_\sigma = 0.92(7)$ . The discrepancy may also be partly explained by applicability problems of the perturbative relation at such large values of  $\kappa$ .

To summarize, both expansions  $\llcorner$  and  $\lrcorner$  work nicely and allow us to extract the low energy constants, in particular  $\Sigma$ , from data on finite lattices.

## 5.2. GOLDSTONE BOSON PROPAGATOR

As may be seen from eqs. (3.19) and (3.24), the wave function renormalization constant  $Z$  [eq. (2.5)] multiplies the leading term of the expression which determines the  $t$ -dependence of  $G_\pi(t)$  in eq. (3.18) or eq. (3.22). This provides a suitable method of extracting precise values of  $Z$ . A preliminary analysis of the data taught us, however, that the chiral perturbation expansion for the propagator on the level of accuracy described in subsect. 3.3 does not work for all our data on small lattices and at lower  $\kappa$  closer to the phase transition. Thus we had to proceed selectively.

For  $\kappa = 0.355, 0.330$  and  $0.325$  we performed the analysis in two steps. In the first step we worked on the  $O(L^{-2})$  level of accuracy, using eq. (3.18) to fit for every data point the last four points of  $G_\pi(t)$ . The coefficients  $a_\pi^0$  and  $b_\pi^0$  were determined by the fit. For each  $\kappa$  we then fitted all  $b_\pi^0$ , except those obtained on the  $8^4$  lattice, by the expression (3.19) using in eq. (3.9) for  $u$  the already known value of  $\Sigma$ . This resulted in an approximate value  $Z_{\text{appr}}$  of  $Z = \Sigma^2/F^2$ .

In the second step we calculated in (3.22) the function multiplying  $1/L^4$  using  $\Sigma$  and  $Z_{\text{appr}}$  and subtracted the values of this term for each  $t$  from the data for  $G_\pi(t)$ . The rest of the data was fitted by the first two terms in eq. (3.22) and the constants  $a_\pi$  and  $b_\pi$  were determined. Their values are given in table 1. Excluding again the  $8^4$  results, the final values of  $Z$  (given in table 2) were extracted from  $b_\pi$  by means of a fit using the expression (3.24) with inserted value of  $\Sigma$ .

In fig. 4 we collect the results for  $b_\pi$  obtained from our data at  $\kappa \geq 0.325$ . The curves represent for each  $\kappa$  the values of the expression (3.22) using the final values of  $\Sigma$  and  $Z$ . They are drawn only in the domain  $\llcorner$ . One can observe that, except for  $\kappa = 0.355$ , the  $8^4$  lattice is too small for the formula (3.22) to be applicable. This is due to the importance of the higher order corrections. On the other hand, on larger lattices the formula (3.22) seems to describe even the data lying outside the domain  $\llcorner$ .

Fig. 5 illustrates the relative importance of the  $1/L^2$  and  $1/L^4$  terms in the formula for the Goldstone propagator (3.22) at  $\kappa = 0.325$  and  $J = 0.0002$  on the

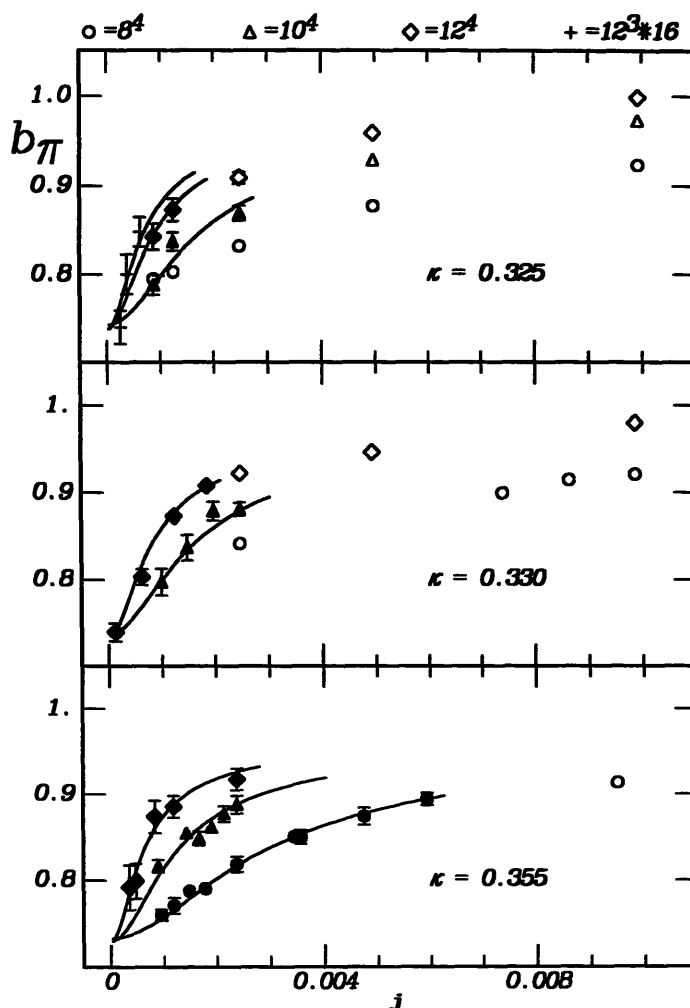


Fig. 4. Values of  $b_\pi$  from a fit to  $G_\pi$  up to order  $1/L^4$ , eq. (3.22). Only the solid symbols have entered the fit of  $b_\pi$  made by means of eq. (3.24). As in fig. 2 the curves displaying the fit are drawn only in the domain  $\mathcal{H}$ .

$12^3 \times 16$  lattice (fig. 5a) and at  $\kappa = 0.33$  and  $J = 0.02$  on the  $12^4$  lattice (fig. 5b). The circles display the data for  $G_\pi(t)$ , which are essentially parabolas with the apex at  $t = L_t/2$ . The triangles have been obtained from the circles by subtracting the  $1/L^2$  term in (3.22) using the value of  $b_\pi$  obtained from the fit. The crosses indicate what remains if the  $1/L^4$  term is subtracted, too. Their positions are in excellent agreement with the values of constant  $a_\pi$ . We conclude that eq. (3.22) describes the data very well and that the  $1/L^4$  term is just a tiny (of the order of 1–2%) correction. This correction is of significance, however, when a precise determination of  $Z$  is required. Particularly remarkable is the negative slope of the triangles (data with the correction  $1/L^2$ ) in fig. 5b which is compensated by the  $1/L^4$  correction. This data point is quite outside the domain  $\mathcal{H}$ , but the expansion  $\mathcal{H}$  still seems to be applicable, as is also indicated by the rapidly decreasing magnitude of the corrections.

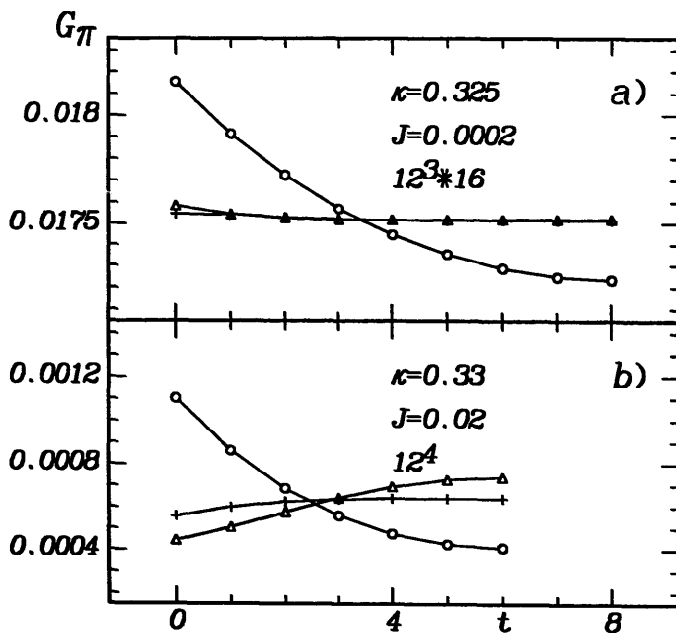


Fig. 5. Relative importance of terms  $O(1/L^2)$  and  $O(1/L^4)$  according to eq. (3.22) in the Goldstone boson propagator. The circles show the measured data for  $G_\pi$ . The triangles have been obtained by subtracting terms  $O(1/L^2)$  of eq. (3.22) from  $G_\pi$ . The crosses result from subtracting also terms  $O(1/L^4)$ . The data point (a) is within and (b) outside the domain  $\mathbb{Z}$ .

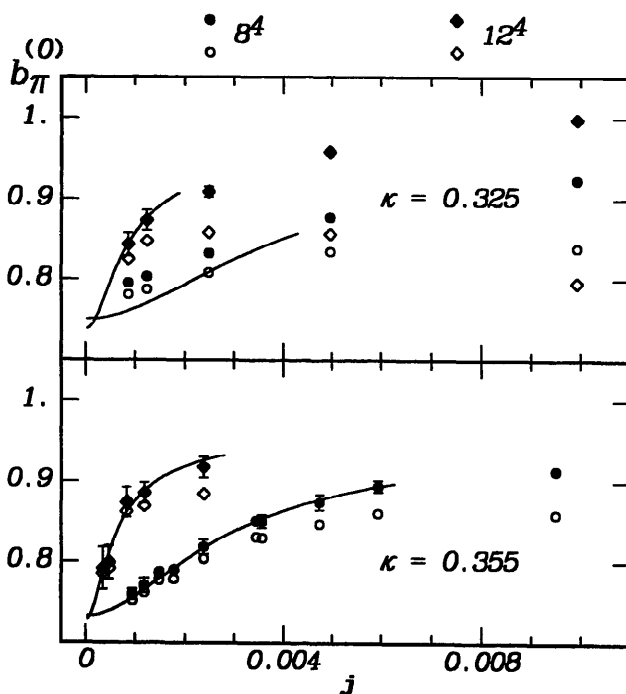


Fig. 6. Analysis of the propagator on two levels of accuracy. Solid symbols are values of  $b_\pi$  from a fit to  $G_\pi$  up to order  $1/L^4$  [eq. (3.22)]. The curves are the fit to these values by means of eq. (3.24). Open symbols are values of  $b_\pi^0$ , eq. (3.18), obtained in the analysis on the accuracy level  $1/L^2$ .

In fig. 6 we give another illustration of the importance of the  $1/L^4$  term in (3.22), this time in more critical situations. We show the values of  $b_\pi^0$ , obtained from the fit to  $G_\pi(t)$  by means of the formula (3.18) (open symbols), as well as  $b_\pi$  obtained using eq. (3.22). The curves are the values of the coefficient (3.24) when the final values of  $\Sigma$  and  $Z$  have been used. For  $\kappa = 0.355$  on the  $8^4$  lattice it is important to take into account the difference between  $b_\pi$  and  $b_\pi^0$  to achieve an agreement with the results obtained on larger lattices. For  $\kappa = 0.325$  on the  $12^4$  lattice both these coefficients agree within the region of validity of the condition (3.6), but start to differ strongly beyond it. Still, the higher order correction improves the agreement with (3.24) significantly.

We have attempted unsuccessfully to analyze the data for the propagator also at the small values of  $\kappa = 0.310$  and  $0.3075$ . As  $M_\sigma$  is rather small (cf. table 2), only the data at large  $t$  can be expected to satisfy the condition (3.5) and to be thus described by chiral perturbation theory. Because of the vicinity to the critical point, the accumulated statistics, similar to the statistics at higher  $\kappa$ , turned out to be insufficient here and the error bars for larger  $t$  were very big. Thus it was only possible to analyze the bulk quantity  $\langle \varphi_x^0 \rangle_{V,j}$ , as described in subsect. 5.1, but not the correlation function.

## 6. Results for vanishing external source

In this section we describe some results of an analysis of the data at  $j = 0$  that we have obtained in part by means of the cluster algorithm [37,38]. Due to this new error-reducing technique the precision of the data allows us to go far beyond the methods used earlier at  $j = 0$  [9–11]. As we are now gaining experience with this approach, the results presented below should be regarded as exploratory.

### 6.1. SUSCEPTIBILITY

Recently it has been pointed out that the moments of the distribution of the magnetization  $|\bar{\varphi}^\alpha|$  (3.2) at  $J = 0$  can be used for extraction of some low energy constants [35]. A first application of this idea has been reported in ref. [34]. We consider the susceptibility  $\chi$  associated with  $|\bar{\varphi}^\alpha|$ . On hypercubic lattices ( $V = L^4$ ) in chiral perturbation expansion it assumes the form

$$\chi = V(\langle |\bar{\varphi}^\alpha|^2 \rangle - \langle |\bar{\varphi}^\alpha| \rangle^2) = \frac{3\Sigma^2}{2F^4} \left[ \beta_2 + \frac{1}{8\pi^2} \ln(\Lambda_\Sigma L) \right], \quad (6.1)$$

where  $\beta_2 = -0.0203$  is a shape coefficient introduced earlier in eq. (3.12). The logarithmic divergence is due to the contribution of the light Goldstone modes. This expression allows the extraction of  $\ln \Lambda_\Sigma$  from the  $L$ -dependence. The susceptibility [eq. (6.1)] has been obtained in our earlier calculations [9,11] for  $J = 0$  at several values of  $\kappa$  for even  $L = 4-16$  (with the Metropolis algorithm) and recently for all  $L = 4-16$  with the cluster algorithm. Here we present a first

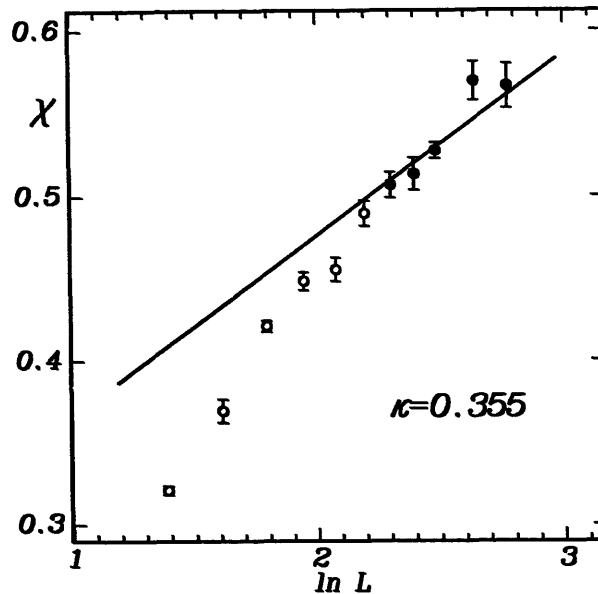


Fig. 7. The susceptibility [eq. (6.1)] as a function of  $\ln L$  on  $L^4$  lattices of size  $L = 4, 5, 6, 7, 8, 9, 10, 11, 12, 14$  and  $16$  at  $\kappa = 0.355$ . The straight line is a fit according to eq. (6.1) for the lattice sizes  $L \geq 10$  (solid circles). It determines the scale parameter  $\Lambda_\Sigma$ .

analysis of these data for  $\kappa = 0.355$  and  $0.33$ . A full account, also including further  $\kappa$  points, will be given elsewhere [40].

In fig. 7 we show data for  $\chi$  at  $\kappa = 0.355$  plotted against  $\ln L$  for  $L = 4-16$ . For small  $L$  the data depart from the linear dependence on  $\ln L$  predicted by formula (6.1). However, for  $L = 10-16$  the increase is consistent with a linear behaviour. Fitting  $\chi$  by means of (6.1) for  $L = 10-16$  and using the known values of  $\Sigma$  and  $F$  we obtain  $\ln \Lambda_\Sigma (\kappa = 0.355) = 3.96(5)$  and  $\ln \Lambda_\Sigma (\kappa = 0.33) = 4.6(2)$  in reasonable agreement with the result obtained in the subject. 5.1, especially if one keeps in mind possible large systematic errors of that determination. We point out that a systematic study of the deviations of  $\chi$  from the linear dependence on  $\ln L$ , aimed for in a separate publication [40], is necessary before the results for  $\ln \Lambda_\Sigma$  may be considered reliable.

Using again the perturbative relationship (3.34) of this parameter to  $M_\sigma$  [31, 39] we obtain for  $M_\sigma$  the preliminary results  $M_\sigma = 1.39(4)$  at  $\kappa = 0.355$  and  $M_\sigma = 0.96(3)$  at  $\kappa = 0.33$ . They are to be compared with the results obtained earlier from the propagator at  $J = 0$  and corrected for finite size effects [12] which are listed in table 2. We note that in the analysis of the propagator the width of the  $\sigma$ -boson has been neglected.

## 6.2. SYMMETRIC PROPAGATOR FOR CYLINDER GEOMETRY

We initiated the study of the model also on elongated lattices  $L_s^3 \times L_t$ , with  $L_t \gg L_s$ , since the cluster algorithm [37, 38] makes the determination of propaga-

tors for such geometry feasible. As has been pointed out in refs. [24,26,28] the most important field modes in this “cylinder” geometry are those with vanishing spatial momentum,  $p = 0$ . Thus the fluctuations in spatial directions may be discarded and only the variation of the field in the time direction of the cylinder is taken into account. In this approximation the system reduces to a quantum mechanical model whose variables are the  $x$ -independent components of the field with values in the manifold of the symmetry group  $O(4)$ . The system may be interpreted as a free quantum mechanical rotator on the  $SU(2) \otimes SU(2)$  manifold and the spectrum, partition function and correlation functions can be calculated using the properties of representations of the  $SU(2)$  group in terms of the low energy constants [26,28].

For the  $O(4)$  symmetric two-point function

$$G(t) = \frac{1}{4L_s^3} \sum_x \langle \varphi_{x,t}^\alpha \varphi_0^\alpha \rangle_{V, j=0} \tag{6.2}$$

one obtains the expression

$$G(t) = \frac{1}{\mathcal{Z}} \frac{\Sigma_L^2}{4} \sum_{n=1}^\infty n(n+1) \exp\left\{ \frac{-L_t}{2F_L^2 L_s^3} \left[ n(n+1) - \frac{1}{2} \right] \right\} \\ \times \cosh\left[ \left( n + \frac{1}{2} \right) \frac{L_t}{F_L^2 L_s^3} \left( \frac{1}{2} - \tau \right) \right] \left[ 1 + O\left( \frac{1}{L^4} \right) \right]. \tag{6.3}$$

Here  $\mathcal{Z}$  is the partition function

$$\mathcal{Z} = \sum_{n=1}^\infty n^2 \exp\left[ \frac{-L_t}{2F_L^2 L_s^3} (n^2 - 1) \right] \tag{6.4}$$

and

$$\Sigma_L = \Sigma \left( 1 + \frac{3\tilde{\beta}_1}{2F^2 L^2} \right), \tag{6.5}$$

$$F_L = F \left( 1 + \frac{\tilde{\beta}_1}{F^2 L^2} \right), \tag{6.6}$$

$$\tilde{\beta}_1 = \beta_1 + \frac{1}{12} \left( \frac{L_t}{L_s} \right)^{3/2}. \tag{6.7}$$

The coefficient  $\beta_1$  is a shape coefficient as defined in subsect. 3.2. We give the values of  $\beta_1$  together with the lattices and  $\kappa$ -values we have used in table 3.

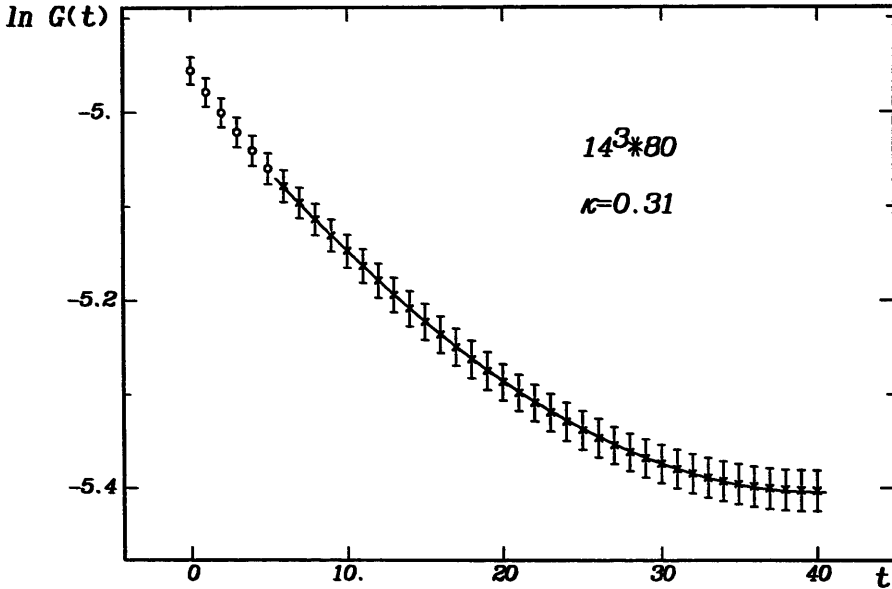


Fig. 8. Example for the  $O(4)$  symmetric two-point function at  $\kappa = 0.31$  on a  $14^3 \times 80$  lattice at  $j = 0$  obtained with the cluster algorithm. The line is a fit made by means of eq. (6.3) for  $6 \leq t \leq 40$  (crosses).

We have analyzed the  $t$ -dependence of  $G(t)$  by means of (6.3); this determines  $F$ . An example of the fit is shown in fig. 8. Typically, for  $L_t = 40$  it is sufficient to take into account 6 (for  $L_s = 8$ ) and 8–9 (for  $L_s = 10$ ) terms of the sum (6.3).

From the data for the correlation function we determine the values of  $F_L$ , from which we then could calculate  $F$ , denoted by  $F_{\text{cyl}}$  in table 3, in order to distinguish it from the determination by means of the expansion  $\mathcal{N}$ . Note the significant dependence of  $F_L$  on the lattice size. This indicates that the  $1/F^2 L^2$  corrections are important. The values of  $F_{\text{cyl}}$  are almost independent of the lattice size. We compare these values with the results of the expansion  $\mathcal{N}$  and find very good agreement at three points  $\kappa = 0.355, 0.320$  and  $0.310$ .

## 7. Conclusions

Our analysis demonstrates, that for  $M_\sigma \gg 1/L$ , i.e. in a situation where the light Goldstone bosons control the dynamics of the system at large distances, it is possible to determine several infinite volume, zero external source quantities from finite volume simulations in a theoretically controlled way. At small values of  $j$ , in the symmetry restoration regime  $\mathcal{N}$ ,  $M_\pi L \lesssim 1$ , the drastic  $j$ - and  $L$ -dependence of  $\langle \varphi_x^0 \rangle_{V,j}$  is well described by the formulas of chiral perturbation theory; this allows a reliable determination of  $\Sigma$ . For sufficiently large lattices and  $\kappa$  values the wave function renormalization constant  $Z$  may be most precisely obtained from the  $t$ -dependence of the Goldstone propagator. We also remark that the values of  $\Sigma$

and  $Z$  obtained in our previous work [9, 11] for a zero external source by means of a global rotation of the configurations are consistent with the present results. Both results have comparable statistical errors, those obtained by means of the  $\mathcal{U}$ -expansion are theoretically more reliable, however.

For larger  $j$ , in the domain  $\mathcal{V}$ ,  $M_\pi L \gtrsim 1$ , the field expectation value follows a different functional behaviour, now well described by the  $\mathcal{V}$  expansion. There one may utilize the knowledge of  $\Sigma$  from the  $\mathcal{U}$ -expansion and fix it in order to obtain the scale parameter  $\ln \Lambda_\Sigma$  which enters in higher order terms of the expansion. There is a substantial overlap between the  $\mathcal{U}$  and  $\mathcal{V}$  region:  $\frac{1}{2} \lesssim M_\pi L \lesssim 1$ .

If  $\kappa$  is close to the critical point, i.e.  $\kappa \lesssim 0.31$  or  $M_\sigma \lesssim 0.39$  the domain  $\mathcal{U}$  shrinks and one needs higher order terms in the expansion. We find differences of 4% between the values of  $\Sigma$  obtained in  $O(L^{-2})$  vs.  $O(L^{-4})$ . Obviously the condition (1.1) gets into trouble and the finite size effects caused by the  $\sigma$ -state become increasingly important.

We also explored alternative methods to determine  $\Sigma$  and  $F$ , or, fixing their values to those obtained in the  $\mathcal{U}$ -expansion, to determine the scale parameter  $\ln \Lambda_\Sigma$ . One is measuring the susceptibility of  $|\bar{\varphi}^\alpha|$ , eq. (6.1), at  $j=0$ . This appears to provide the best way to get  $\ln \Lambda_\Sigma$  with smallest statistical error. As this parameter may be related to the mass  $M_\sigma$  by a weak coupling expansion, the method allows us to determine this mass from a bulk quantity.

In cylinder geometry, again at  $j=0$ , the cluster algorithm enabled us to determine the  $O(4)$ -invariant propagators at large distances. Its shape may be understood with help of a quantum mechanical rotator approximation where once again the low energy parameters  $\Sigma, F$  enter. From the decay behaviour one may determine  $F$ , and we find good agreement with the other results. Whereas we had the possibility to check the convergence properties and the systematic error in the  $\mathcal{U}$  expansion, we are not in this situation here, unfortunately.

Altogether we find that the volume dependence of the field expectation value and the correlation functions are excellently described by the chiral perturbation expansion. At small  $M_\sigma$  one has to include higher order terms and eventually will run into convergence problems. Away from the critical point, deeper in the broken phase, our study demonstrates that the chiral expansion provides a simple and reliable method to find the (infinite volume,  $j \rightarrow 0$ ) low energy constants  $\Sigma, F$  (or  $Z$ ) from finite volume results. On a lower accuracy level the method is very simple. When higher order corrections are to be taken into account, the complexity of the data analysis increases substantially, though the method is, in principle, straightforward. We hope that the method will prove to be as useful in lattice QCD as it has turned out to be for the study of the Higgs sector of the standard model.

Our precise determination of  $F$  continues our study [9, 11, 12, 32] of the upper bound on the Higgs boson mass in the spirit of ref. [1]. To accomplish this a reliable determination of  $M_\sigma$  from the data obtained on finite lattices is required. This question will be addressed in a forthcoming work [40].

We appreciate helpful suggestions of P. Hasenfratz and discussions with M. Göckeler. T.N. acknowledges the kind hospitality of SCRI given to him. The research of A.H. was partially supported by the Florida State University Super-computer Computations Research Institute which is partially funded by the US Department of Energy through Contract No. DE-FC05-85ER250000. J.J. was partially supported by the Deutsches Bundesministerium für Forschung und Technologie. C.B.L. acknowledges the support of Jubiläumsfonds der Österreichischen Nationalbank. T.N. acknowledges partial support from the Department of Energy through Contracts DE-FG05-87ER4031 and DE-FC05-85ER250000.

The computations were performed on the ETA10 of SCRI at Florida State University, on the CRAY X-MP/416 and CRAY Y-MP/832 at HLRZ Jülich and on the Convex C240 of the University of Bielefeld.

### References

- [1] R. Dashen and H. Neuberger, *Phys. Rev. Lett.* 50 (1983) 1897
- [2] A. Hasenfratz and P. Hasenfratz, *Phys. Rev.* D34 (1986) 3160
- [3] H. Neuberger, in *Lattice Higgs workshop*, ed. B. Berg et al. (World Scientific, Singapore, 1988) p. 197
- [4] P. Hasenfratz, *Nucl. Phys. B (Proc. Suppl.)* 9 (1989) 3
- [5] J. Kuti, in *Proc. XXIV. Int. Conf. on HEP, Munich, 1988*, ed. R. Kotthaus and J.H. Kühn (Springer, 1989)
- [6] J. Jersák, in *Higgs particle(s) – physics issues and searches in high energy collisions*, Erice Workshop (July 1989), ed. A. Ali (Plenum, New York, 1990) p. 39
- [7] P. Hasenfratz and J. Nager, *Z. Phys.* C37 (1988) 477
- [8] M. Lüscher and P. Weisz, *Phys. Lett.* B212 (1988) 472; *Nucl. Phys.* B318 (1989) 705
- [9] A. Hasenfratz, K. Jansen, C.B. Lang, T. Neuhaus and H. Yoneyama, *Phys. Lett.* B199 (1987) 531
- [10] J. Kuti, L. Lin and Y. Shen, *Nucl. Phys. B (Proc. Suppl.)* 4 (1988) 397; *Phys. Rev. Lett.* 61 (1988) 678; in *Lattice Higgs workshop*, ed. B. Berg et al. (World Scientific, Singapore, 1988) p. 140; J. Kuti, L. Lin, Y. Shen and S. Meyer, in *Lattice Higgs workshop*, ed. B. Berg et al. (World Scientific, Singapore, 1988) p. 216
- [11] A. Hasenfratz, K. Jansen, J. Jersák, C.B. Lang, T. Neuhaus and H. Yoneyama, *Nucl. Phys.* B317 (1989) 81; K. Jansen, *Nucl. Phys. B (Proc. Suppl.)* 4 (1988) 422; C.B. Lang, in *Lattice Higgs workshop*, ed. B. Berg et al. (World Scientific, Singapore, 1988) p. 158
- [12] T. Neuhaus, *Nucl. Phys. B (Proc. Suppl.)* 9 (1989) 21
- [13] J. Kuti, L. Lin and Y. Shen, *Nucl. Phys. B (Proc. Suppl.)* 9 (1989) 26
- [14] H. Neuberger, *Phys. Lett.* B199 (1987) 536; G. Bhanot, K. Bitar, U.M. Heller and H. Neuberger, *Nucl. Phys.* B343 (1990) 467; RU-90-35
- [15] G. Bhanot and K. Bitar, *Phys. Rev. Lett.* 61 (1988) 798; in *Lattice Higgs workshop*, ed. B. Berg et al. (World Scientific, Singapore, 1988) p. 21
- [16] H. Neuberger, *Nucl. Phys. B (Proc. Suppl.)* 17 (1990) 17
- [17] U. Heller, *Nucl. Phys. B (Proc. Suppl.)* 17 (1990) 649
- [18] C.B. Lang, *Phys. Lett.* B229 (1989) 97; *Nucl. Phys. B (Proc. Suppl.)* 17 (1990) 665
- [19] C. Frick, K. Jansen, J. Jersák, I. Montvay, G. Münster and P. Seufferling, *Nucl. Phys.* B331 (1990) 515
- [20] M. Lüscher, *Commun. Math. Phys.* 105 (1986) 153
- [21] W. Langguth and I. Montvay, *Z. Phys.* C36 (1987) 725; A. Hasenfratz and T. Neuhaus, *Nucl. Phys.* B297 (1988) 205
- [22] H.G. Evertz, E. Katznelson, P.G. Lauwers and M. Marcu, *Phys. Lett.* B221 (1989) 143

- [23] M.E. Fisher and V. Privman, *Phys. Rev.* B32 (1985) 447; *Commun. Math. Phys.* 103 (1986) 527; *J. Mag. Mag. Mat.* 54–57 (1986) 663
- [24] E. Brézin, *J. Phys. (Paris)* 43 (1982) 15;  
E. Brézin and J. Zinn-Justin, *Nucl. Phys.* B257 [FS14] (1985) 867
- [25] J. Gasser and H. Leutwyler, *Phys. Lett.* B184 (1987) 83; B188 (1987) 477
- [26] H. Leutwyler, *Phys. Lett.* B189 (1987) 197
- [27] J. Gasser and H. Leutwyler, *Nucl. Phys.* B307 (1988) 763
- [28] H. Leutwyler, *Nucl. Phys. B (Proc. Suppl.)* 4 (1988) 248
- [29] H. Neuberger, *Phys. Rev. Lett.* 60 (1988) 889; *Nucl. Phys.* B300 [FS22] (1988) 180; *Nucl. Phys. B (Proc. Suppl.)* 4 (1988) 501
- [30] P. Hasenfratz and H. Leutwyler, *Nucl. Phys.* B343 (1990) 241
- [31] J. Gasser and H. Leutwyler, *Ann. Phys. (N.Y.)* 158 (1984) 142
- [32] A. Hasenfratz, K. Jansen, J. Jersák, C.B. Lang, H. Leutwyler and T. Neuhaus, *Z. Phys.* C46 (1990) 257
- [33] U.M. Heller and H. Neuberger, *Phys. Lett.* B207 (1988) 189
- [34] T. Neuhaus, Talk at the Int. Workshop, Lattice 89, in Capri, Italy (Sept. 1989) (unpublished)
- [35] M. Göckeler, *Nucl. Phys. B (Proc. Suppl.)* 17 (1990) 347;  
M. Göckeler and H. Leutwyler, *Nucl. Phys.* B350 (1991) 228; *Phys. Lett.* B253 (1991) 193
- [36] E. Brézin, J.C. Le Guillou and J. Zinn-Justin, in *Phase transitions and critical phenomena*, vol. 6., ed. C. Domb and M.S. Green (Academic Press, New York, 1976)
- [37] U. Wolff, *Phys. Rev. Lett.* 62 (1989) 361;  
C. Frick, K. Jansen and P. Seufferling, *Phys. Rev. Lett.* 63 (1989) 2613
- [38] K. Jansen, *Nucl. Phys. B (Proc. Suppl.)* 17 (1990) 289
- [39] M. Göckeler, private communication
- [40] M. Göckeler, K. Jansen and T. Neuhaus, to be published